Sharshir *et al.*
Journal of Analytical Science and Technology (2022) 13:16
https://doi.org/10.1186/s40543-022-00326-5

Journal of Analytical Science and Technology

RESEARCH ARTICLE Open Access

Experimental investigation of E-beam effect on the electric field distribution in cross-linked polyethylene/ZnO nanocomposites for medium-voltage cables simulated by COMSOL Multiphysics

A. I. Sharshir[1*], S. A. Fayek[1], Amal. F. Abd El-Gawad[2], M. A. Farahat[2], M. I. Ismail[2] and Mohamed Mohamady Ghobashy[3]

Abstract

This study investigated the electric field distribution of underground cable insulation in cross-linked polyethylene/zinc oxide (XLPE/ ZnO) nanoparticles (NPs) for medium-voltage (MV) cables. The ZnO NPs that were obtained by three methods of preparation were classified using transmission electron microscopy (TEM). The obtained ZnO NPs were semi-spheres with sizes of 35–55 nm on TEM images. XLPE/ ZnO films with various ZnO NP weight contents (i.e., 0, 1, 3, and 5%) were exposed to varied dosages of 3-MeV electron beam (EB); 0 kGy, 15 kGy, 20 kGy, and 25 kGy. The optimum film XLPE/ 5-ZnO, which has ZnO NP content (5 wt%), irradiated at 25 kGy, according to alternating current (AC)/ DC conductivity (AC: 1×10^{-4} S/m; DC: 12.44×10^{-2} S/m) in minimum relative permittivity (2.24), was obtained. COMSOL Multiphysics was used to simulate the electric field distribution within an MV cable of 25-kGy XLPE/ 5-ZnO insulation. The maximum uniform electric field was found in the middle of the 25-kGy XLPE/5-ZnO film sample, rather than at the top or bottom, which might be attributed to the significantly low relative permittivity of the new 25-kGy XLPE/5-ZnO film cable.

Keywords: Cross-linked polyethylene cable, Electron beam irradiation, COMSOL Multiphysics, Zinc oxide NPs

Introduction

Cross-linked polyethylene, commonly abbreviated as XLPE, is composite of polyethylene plastic with cross-links (Morshedian and Mohammad 2009). Predominantly, XLPE is used in high- and medium-voltage electrical cables because XLPE has impact strength of low temperature, abrasion resistance, and cracking resistance (Aljoumaa and Allaf 2021). Compared to thermoplastic polyethylene, XLPE is thermally resistant even at higher temperatures (Oliveira and Costa 2010). Sometimes XLPE thermal and electrical properties significantly increased when XLPE is supported with a metal or metal oxide (Thomas et al. 2019).

According to their outstanding electrical, thermal, mechanical, and chemical characteristics, nano-fillers, such as ZnO, have received so much interest in further strengthening composites. The addition of ZnO to a polymer matrix can improve load transmission and composite strength (Oliveira and Costa 2010; Thakur et al. 2020). As a result, by incorporating nano-fillers into current polymer systems, composite performance and application range can be enhanced (Makhado et al. 2020).

*Correspondence: a.shr88@yahoo.com

[1] Solid State and Accelerator Department, National Center for Radiation Research and Technology (NCRRT), Egyptian Atomic Energy Authority (EAEA), Cairo, Egypt
Full list of author information is available at the end of the article

Nano-fillers are particularly important in the development of polymer nanocomposites due to its intrinsic properties. Some NPs, e.g., ZnO have outstanding stability, a high refractive index, hydrophilicity, ultraviolet (UV) resistance, great transparency to visible light, non-toxicity, strong photocatalytic activity, and low cost. ZnO may be made into various nano-structures, including nano-rods, nanowires, spherical NPs, and tetra pods, and is a multi-functional n-type (II–V) semiconductor with a large binding energy (60 meV), excellent UV absorbance, and a broadband gap (3.4 eV) (Janotti and Walle 2009; Hezam et al. 2018). ZnO NPs have unique properties allowing them to exist in either an anti-electrostatic or conductive state. In the literature, the electrical (Patil et al. 2013), magnetic (Yılmaz et al. 2013), chemical (Suwanboon et al. 2014), and optical (Labuayai et al. 2009) properties of ZnO NPs are remarkable. It has been used in catalysis and semiconductor manufacturing (Ko et al. 2003; Zaouk et al. 2006). From a literature review, it was found that various approaches for preparing ZnO nano-powders have been developed, namely, sol–gel (Kumar et al. 2020), microemulsion (Pifferi et al. 2015), thermal decomposition of organic precursor (Simonenko et al. 2018), spray pyrolysis (Sree et al. 2019), electrodeposition (Prasad et al. 2020), ultrasonic (Fattahi and Pak 2018), microwave-assisted techniques (Garino et al. 2019), chemical vapor deposition (Mohammed and Hassan 2019), and hydrothermal and precipitation methods. Based on the above synthetic methods, this paper developed and modified another new three methods of ZnO nanoparticles preparation, e.g., using oxalic acid, metal precipitation, and metal displacement.

The technique of electron beam (EB) irradiation has become an advanced method recently to improve the physical properties of materials, such as conductivity and mechanical, structural, and thermal stability. As gamma irradiation, the EB energy interacts with polymer material, it causes molecular structural changes (Ghobashy et al. 2018a), such as ionization, atom displacement, carbonization, and the production of free radicals, contributing to chain scission and cross-linking reactions (Ghobashy et al. 2020). As a result, polymer modification has become an important research topic (Ghobashy et al. 2018b; Younis et al. 2020), particularly in industrial applications, including wire, cable, electronic devices, medical, and marine. Radiation can only change the chemical composition of the polymer (Ghobashy et al. 2021); however, it may also increase the presence of trapped charges or cause defects in the matrix (Raghu et al. 2014). This structural change in the irradiated polymer electrolyte has a direct impact on physical properties; in this case, dielectric permittivity and electrical conductivity improved as the dose was increased. The physics and chemistry of the absorbed products, as well as the chosen radiation energy and dose as a result of cross-linking or chain scission, influence the aforementioned changes. The induced radiation affected the presence of trapping charge within the material, increasing the transport property. It has also been observed that changing the functional group of a polymer changes the physical properties of polymer films. As a result, changes in the dielectric, electrical, and thermal properties of irradiated polymers can be attributed to these changes (Wei and Zhu 2020; Raghu et al. 2016). In other words, irradiated polymers can be converted from insulators to materials with good electrical conductivity, which is a good sign since these materials can be used in various electronic applications. Sharshir et al. (2021) have used a melt mixer to prepare XLPE cables composited with copper NPs (CuNPs). Different NP ratios were used to make the XLPE/ Cu nanocomposites (i.e., 0, 1, 3, and 5 wt%) at different EB irradiation doses of 0, 15, 20, and 25 kGy. In a frequency range of 50 Hz–1.5 MHz, the relative permittivity (ε_r), dielectric′ constant (ε'), dielectric loss factor (ε''), and conductivity (tan) were calculated. The improvement in the electric field uniform occurs in the middle of the 25-kGy XLPE/5-ZnO film cable that has a CuNP content of 5 wt% and irradiated at 25 kGy.

Kim et al. (2019) have highlighted in a recent study that the undertaken modifications in the chemical and physical structures of XLPE insulation behavior, under thermal aging, lead to many changes in the dielectric characteristics of XLPE. The mechanical properties of XLPE decreased. From another viewpoint, the leakage current can be considered an important indicator of high-voltage insulation degradation. Moreover, the leakage current can flow through the surface and/ or bulk of the materials, and this current can have a solid relation with the aging process. Lei et al. (2017) have examined the preparation of XLPE/silicon dioxide (SiO_2) nanocomposites, which used DC currents. The strength of the nano-breakdown composite was considerably greater than that of the unfilled XLPE in the DC phase test. The difference between the typical lives of the nanocomposite and its empty base polymer dropped when the applied field was reduced, and the lifetimes were relatively similar when the applied field was 130 kV/mm, according to endurance tests.

Here, XLPE/ZnO nanocomposites were thoroughly investigated according to the impact of various contents of ZnO on XLPE polymers, including simulating the electric field distribution. The XLPE/ZnO nanocomposites irradiated with EB were simulated using the COMSOL Multiphysics program. The first part of this study is about the preparation and characterization of ZnO NPs. The second part explains the simulation steps and shows how

electric field strength propagates in ZnO NPs filled with XLPE medium-voltage (MV) cables. When ZnO NPs were filled into XLPE, they increased conductivity and decreased permittivity, resulting in a uniform electric field arising from the current flow via MV cables.

Material and experimental section

XLPE pellets were supplied by El Sewedy, Giza Cables Company, Egypt. They were used for XLPE MV cable manufacture (33 kV). Zinc acetate dihydrate $Zn(CH_3COO)_2{\cdot}2H_2O$ with purity of 98%, oxalic acid (OX) ($C_2H_2O_4$) with purity of 98%, and ammonium hydroxide (NH_4OH) 30 wt% were supplied by Sigma-Aldrich (Missouri, USA). The typical procedures for preparing ZnO NPs using three methods are outlined as follows:

Oxalic acid (OX) method ((ZnO)OX)

Zinc acetate dehydrate ($Zn(CH_3CO_2)_2{\cdot}2H_2O$) (1 M) and oxalic acid $C_2H_2O_4$ (1 M) were separately dissolved in distilled water to form homogenous solutions of (A) and (B), respectively. (A) and (B) were mixed thoroughly under vigorous stirring conditions for 30 min and under sonication at ambient temperature up to the formation of white precipitate of zinc oxalate dehydrate ($ZnC_2O_4{\cdot}2H_2O$). The precipitate was then washed several times with distilled water and dried in an oven at 100 °C for 2 h to remove water, followed by heat treatment at 800 °C for 2 h to obtain a fine powder of Zn metal. The samples were structurally and morphologically examined using an X-ray powder diffractometer. The reactions for the formation of zinc oxalate dehydrate from the salts were as follows:

$$ZnSO_4 \cdot 7H_2O\ (sol) + C_2H_2O_4\ (sol) \rightarrow ZnC_2O_4 \cdot 2H_2O\ (ppt) + H_2SO_4 + 5H_2O \quad (1)$$

$$Zn(NO_3)2 \cdot 7H_2O\ (sol) + C_2H_2O_4(sol) \rightarrow ZnC_2O_4 \cdot 2H_2O(ppt) + 2HNO_3 + 5H_2O \quad (2)$$

$$ZnCl_2 \cdot 4H_2O\ (sol) + C_2H_2O_4(sol) \rightarrow ZnC_2O_4 \cdot 2H_2O(ppt) + 2HCl + 2H_2O \quad (3)$$

$$ZnC_2O_4 \cdot 2H_2O\ (ppt) \rightarrow Zn + 2CO_2 + 2H_2O \quad (4)$$

$$Zn + (O_2)\ air \rightarrow ZnO. \quad (5)$$

Metal displacement reaction (MDR) method ((ZnO)MDR)

An appropriate weight of aluminum (Al) powder was added to the $Zn(CH_3CO_2)_2{\cdot}2H_2O$ solution. The reaction stood for 24 h under sonication conditions. The color changes in the $Zn(CH_3CO_2)_2{\cdot}2H_2O$ solution indicated the beginning of Zn metal formation.

Metal oxide precipitation (MOP) method ((ZnO)MOP)

NH_4OH was added drop by drop to the $Zn(CH_3CO_2)_2{\cdot}2H_2O$ solution until it provides gelatinous weight precipitates of zinc hydroxide. The precipitate was washed several times with distilled water and dried in an oven at 100 °C for 2 h to remove water, followed by heat treatment at 800 °C for 2 h to obtain a fine powder of Zn metal.

AC and DC conductivity of different contents of ZnO NP-filled XLPE

The I–V characteristics (ZnO NPs/XLPE) of the sample were measured at room temperature. We used Keithley source measure units (model 2635A) to measure the *I–V* characteristics, which were regulated by specially designed ACS Basic Software (Keithley). The LCR bridge model Hioki 3532 was used to measure the sample (ZnO NPs/XLPE) impedance Z and the phase angle between the applied AC voltage and the resulting current in the sample (ZnO NPs/XLPE) for AC conductivity measurement $\sigma_{AC}(\omega)$. The frequency ranged from 50 Hz to 1.5 MHz (0.05:1500 kHz).

The variation in AC conductivity with a frequency at ambient temperature was examined on the ln–ln scale. The variance of AC and DC with a frequency ranging from 50 Hz to 1.5 MHz was studied for the investigated compositions (all of which had the same thickness; 5 mm). At various ZnO NP concentrations, the obtained results were plotted as $\ln \sigma_{AC}(w)$ versus $\ln w$.

The sample impedance (Z), sample capacitance (C_p), and loss tangent ($\tan\delta$) were directly measured using a programmable automatic 3532 LCR meter. The resistance R was parallel to all values of C_p, which was taken from the bridge's screen. The equation used to calculate the total conductivity σt (w) was as follows:

$$\sigma_t(w) = L/ZA,$$

where L is the distance between the two electrodes (the sample thickness), Z is the impedance of the sample, and A is the cross-sectional area of the sample. Using the

relation, the AC conductivity (σAc(w)) is calculated as follows:

$$\sigma_{Ac}(w) = \sigma_t(w) - \sigma_{DC}(w)$$

where $\sigma_{DC}(w)$ is termed as the DC conductivity.

Preparation of (XLPE/ZnO) nanocomposites

Before mixed process, XLPE pellets and ZnO nanoparticles powder were dried overnight at 70 °C in an oven remove excess moisture. The XLPE pellets were mixed with weight contents of ZnO nanoparticles (0, 1, 3, and 5 wt%) using a mechanical mixer. The mixing process was carried out at temperature of 170 °C under a rotor speed of 120 rpm and the mixing time is 5 min. Then, the meld (XLPE/ ZnO) samples were molded using the rectangle mold which was heated to 190 °C and were held for 5 min under a mechanical press to be fully melted. The tableting machine pressure was kept at 10 MPa and the mold temperature was decreased to 50 °C for 5 min. The tableting machine pressure and the mold temperature was decreased to the ambient pressure and temperature, respectively. The mixing and molding process was the same procedure as the blank sample was prepared. Then, all samples are exposed to different electron beam irradiation doses of (0, 15, 20, and 25 kGy).

Composite irradiation

A linear particle accelerator (Vivi rad company, France) of 3.0 MeV electron flux with 30 mA at rated current and conveyor speed 16 m/min was used for the irradiation of the samples. The dimension of source electron beam accelerator was (80 × 70 cm). The minimum dose was 3 kGy. The dose rate depended on conveyor speed and current. The films were irradiated at ambient temperature by accelerated electrons until the absorbed doses of 15 and 25 kGy were reached.

Simulation procedure of electric field distribution

The electric field distribution was studied starting from the copper core to the outer semiconductor layer of the cable. The cable layers were subjected to a constant 2Uo = 24 kV 50 Hz AC power supply (where Uo is the cable's rated line to neutral voltage). The electric fields effects were then investigated using COMSOL Multiphysics.

As a compression sample in this study, the XLPE-marked cable used was a single-core 22 kV shielded underground cable. The copper conductor with a 4.165 mm radius, inner semiconductor of 4.95 mm, XLPE insulation of 10.45 mm, and outer semiconductor of 11.25 mm are useful layers used in the analysis. All radii have been estimated from the middle of the copper conductor.

Characterization of zinc oxide nanoparticles

Ultraviolet–visible spectrophotometer (Ultraviolet-3600, Shimadzu) was utilized to monitor the characterization of the synthesized ZnO nanoparticles at a scanning range of 200–700 nm, and autoclaved gum utilized as a blank. The Fourier transform infrared spectroscopy (FTIR/ATR) is a technique used to obtain an infrared spectrum of solid samples of ZnO nanoparticles. The powder-XRD technique was utilized by *XRD*-7000 Shimadzu, Germany. The process for crystalline analysis of the ZnONPs with Cukα radiation ($\lambda = 1.5418$ Å) Shimadzu. The TEM has used to determine the size and morphology of the prepared ZnONPs. The sample grid was primed for TEM calculation by inserting a drop in aqueous ZnONPs dispersion in acetone solvent on the carbon-coated copper grid, and then evaporating the water spontaneously overnight under atmospheric conditions.

Results and discussion

The physicochemical properties of ZnO NPs prepared using three preparation methods

X-ray diffraction (XRD) was used to differentiate between ZnO nanoparticles obtained using the three methods and the presence of ZnO_2 NPs. Figure 1a shows the XRD patterns of ZnO NPs obtained using the (ZnO)OX, (ZnO)MDR, and (ZnO)MOP methods, which displayed peaks of both ZnO and ZnO_2 NPs on XRD according to the International Center for Diffraction Data (ICDD) (89-1397 and 77-2414, respectively). All ZnO NP samples were in the crystalline form (Fig. 1a). For the (ZnO)OX sample, three distinct XRD peaks were found located at $2\theta = 31.68°$, 34.34°, and 36.17°, which corresponded to the lattice patterns of 100, 002, and 101 face-centered cubic of pure ZnO NPs, respectively, and six intensity peaks were displayed located at $2\theta = 47.47°$, 56.53°, 62.79°, 66.27°, 67.88°, and 69.02°, which corresponded to ZnO NPs (Singh and Vishwakarma 2015). For the (ZnO)MDR sample, 10intensity peaks were found located at $2\theta = 31.65°$, 34.28°, 36.13°, 47.46°, 56.52°, 62.76°, 66.27°, 67.86°, 69.01°, and 72.17°, which corresponded to ZnO NPs. These peaks fully fit File ICDD No. 89-1397, which confirmed the creation of pure crystal ZnO NPs. The two weak-intensity peaks located at $2\theta = 78.09°$ and 81.47° corresponded to ZnO_2 NPs according to File ICDD No. 77-2414. For the (ZnO)MOP sample, the XRD curve showed seven intensity peaks located at $2\theta =$ at 31.83°, 34.56°, 36.34°, 47.66°, 56.65°, 68.04°, and 69.14°, which corresponded to ZnO NPs according to File ICDD No. 89-1397. The two weak-intensity peaks located at $2\theta = 63.02°$ and 66.44° corresponded to ZnO_2 NPs according to File ICDD No. 77-2414. The percentage

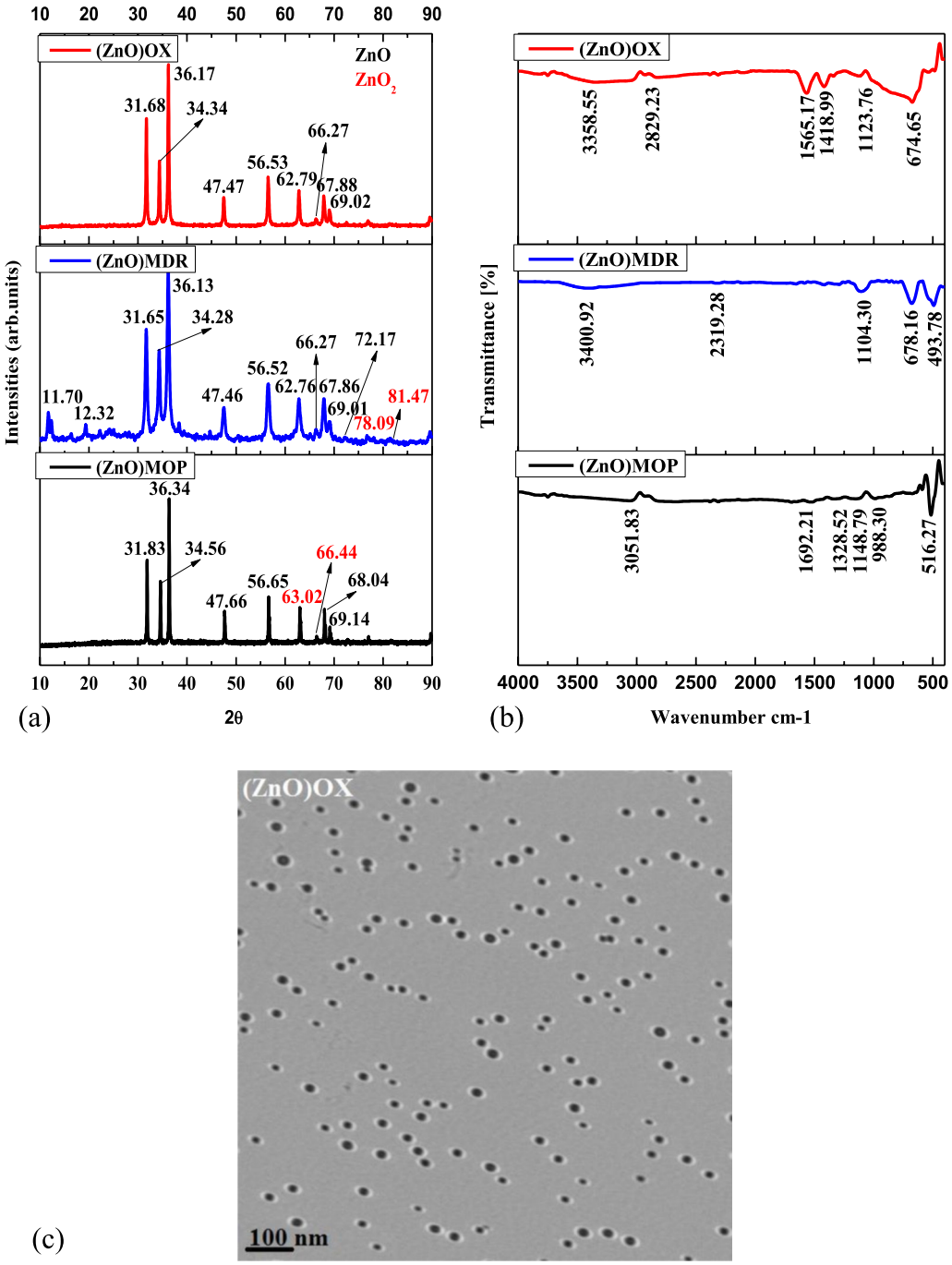

Fig. 1 **a** X-ray diffraction spectra and **b** Fourier transform infrared spectroscopy spectra were obtained using the three preparation methods. **c** Transmission electron microscopy images of zinc oxide (ZnO) nanoparticles obtained using the oxalic acid ((ZnO)OX)) method

of NP structures in ZnO was verified using XRD pattern analysis. Consistent with the XRD data, such as the intensity of peaks, Table 1 shows that ZnO NPs were the most abundant phase in the (ZnO)OX sample (100%), followed by (ZnO)MDR and (ZnO)MOP with the content of 97.97% and 89.63%, respectively, whereas ZnO_2 was the most abundant phase in the (ZnO)MDR sample (2.03%), and ZnO_2 was the most abundant phase in the (ZnO)MOP sample (10.37%). These data confirm that (ZnO)OX is an abbreviated technique for preparing pure ZnO NPs. Almost, the XRD pattern at $2\theta \sim 34$, 36, and 47 corresponding to (0 0 2), (1 0 1), and

Table 1 X-ray diffraction analysis of the zinc oxide (ZnO) nanoparticle (NP) samples prepared using three methods (ZnO) OX, (ZnO)MDR, and (ZnO)MOP) showing the variation in ZnO NP content according to the preparation method used

Sample	ZnO%	ZnO_2%
(ZnO)OX	100	0
(ZnO)MDR	97.97	2.03
(ZnO)MOP	89.63	10.37

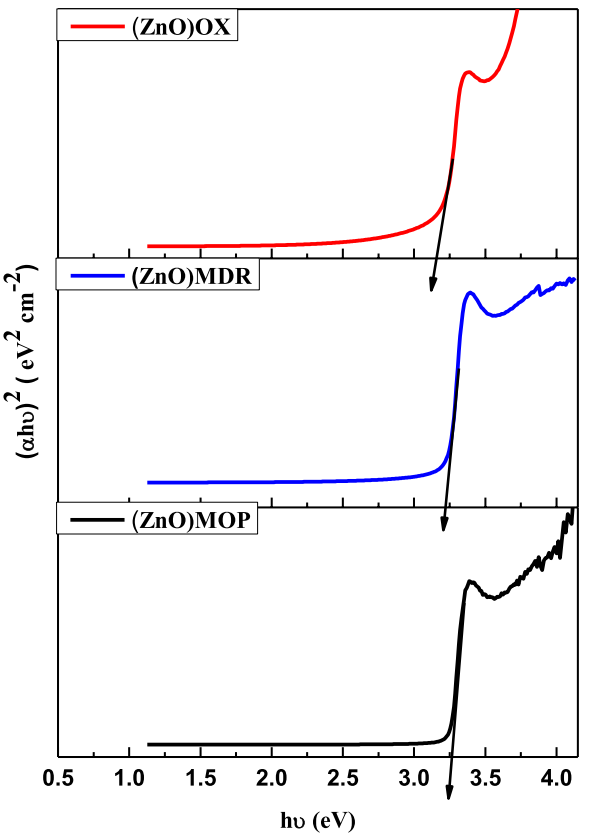

Fig. 2 The calculation of the band gap energy of zinc oxide (ZnO) nanoparticles

(1 0 2) lattice planes of obtained ZnO has been indexed as a hexagonal unit cell (Mututu et al. 2019; Mahmood et al. 2021).

Figure 1b represents the Fourier transform infrared spectroscopy (FTIR) spectra of ZnO NPs obtained from three preparation methods, such as (ZnO)OX, (ZnO) MDR, and (ZnO)MOP. These FTIR spectra revealed a peak located at ~ 600 cm^{-1} that attributed to ZnO bonds, and the FTIR peak located at ~ 870 cm^{-1} was attributed to Zn–OH bonds (Moniri et al. 2017). It is clear from Fig. 2b that Zn–O bonds exist in all ZnO NP samples, and Zn–OH bonds are present in the ZnO sample only.

Table 2 Optical band gap of zinc oxide nanoparticles obtained using different preparation methods

Sample	(ZnO)OX	(ZnO)MDR	(ZnO)MOP
Optical band gap (E_g)	3.12	3.2	3.3

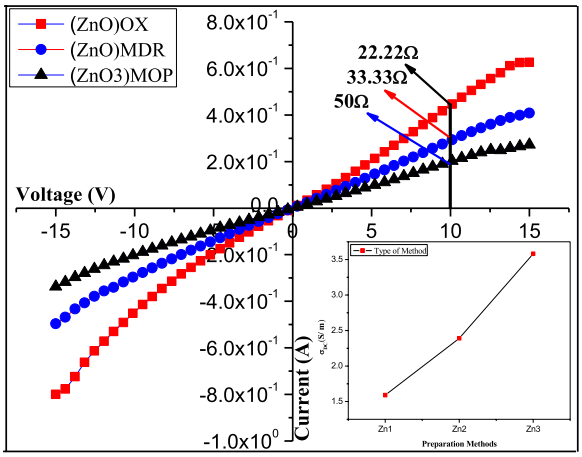

Fig. 3 *I–V* curve of (ZnONPS). The inner curve shows the electrical conductivity of ZnO NPs obtained using the three preparation methods

Figure 1c represents the TEM image of ZnO NPs prepared using the OX method ((ZnO)OX). These ZnO NPs obtained using the (ZnO)OX method were almost spherical in shape, and their morphology was the same with a mean size of 35 nm ± 10 nm because the creation of ZnO NPs was quick without agglomeration observation (Fig. 1c).

The three band gaps of ZnO NPs (i.e., (ZnO)OX, (ZnO)MDR, and (ZnO)MOP) are shown in Fig. 2. The band gaps ranged from 3.12 to 3.3 eV since the values depended on several factors, such as the particle size and purity of the ZnO produced. Table 2 shows how to determine the band gap, for example, by extending the straight part to the energy axis at (alpha)2 = 0. When it can be observed, the band gap increased as the oxidation of ZnO occurs (Fayek et al. 2018).

I–V characteristics curve of ZnO NPs prepared using the three methods

The I–V characteristic curves of the ZnO NPs prepared using three methods (ZnO)OX, (ZnO)MDR, and (ZnO) MOP) are shown in Fig. 3. In the *I–V* curves, ohmic behavior was observed in ZnO NPs prepared using the three methods. In the first and third quarters, the *I–V* characteristics were nearly symmetrical, confirming the same resistance. Table 3 shows that the resistance of ZnO

Table 3 The resistance and conductivity of zinc oxide nanoparticles obtained using the three preparation methods

Sample	Resistance (Ω)	Conductivity (S/m)
(ZnO)OX	22.22	3.58
(ZnO)MDR	33.33	2.39
(ZnO)MOP	50	1.59

NPs prepared using the three methods is equal to 22.22, 33.33, and 50Ω, respectively. The resistance of ZnO NPs prepared using the ZnO1 method was lower than that of ZnO NPs prepared using other methods (i.e., ZnO2 and ZnO3). The conductivity of ZnO NPs was measured using the three preparation methods, which equaled 3.58, 2.39, and 1.59 S/m, respectively (Table 3). The conductivity of ZnO NPs prepared using the (ZnO)OX method was higher than that of ZnO NPs prepared using other methods (i.e., (ZnO)MDR and (ZnO)MOP because of the increased conductivity with decreasing oxidation. The ZnO NPs prepared using the OX method will be used in the electric field distribution study of the XLPE/ ZnO nanocomposite system based on the aforementioned results.

The effect of EB irradiation doses on the I–V characteristic curve of XLPE/ZnO-5 nanocomposites

The I–V characteristic curves of XLPE/ ZnO irradiated with four doses of EB at 0, 15, 20, and 25 kGy at 5% ZnO–OX concentration are shown in Fig. 4a. In the *I–V* curves, ohmic behavior was observed in XLPE/5-ZnO. In the first and third quarters, the *I–V* characteristics were nearly symmetrical, confirming the same resistance. Figure 4b shows that the resistance of XLPE/5-ZnO irradiated at 0, 15, 20, and 25 kGy was equal to 2.67×10^3, 1.60×10^3, 1.45×10^3, and $0.64 \times 10^3\Omega$, respectively. The resistance of XLPE/5-ZnO irradiated at 25 kGy was lower than that of XLPE/5-ZnO irradiated at 0, 15, and 20 kGy). Then, the conductivity of XLPE/5-ZnO irradiated at 0, 15, 20, and 25 kGy) was 2.98×10^{-2}, 4.97×10^{-2}, 5.49×10^{-2}, and 12.44×10^{-2} S/m, respectively. The resistance of XLPE/5-ZnO at 25 kGy was the lowest, whereas the conductivity of ZnO NP-filled XLPE at 25 kGy and concentration of 5% ZnO–OX were the greatest, according to the aforementioned results. The conductivity increased 16 times from o to 25 kGy.

AC conductivity measurement for irradiated XLPE/ZnO nanocomposites

The variations in AC conductivity as a function of ln (*f*) for irradiated (XLPE/ZnO) nanocomposites with various ZnO contents (i.e., 0, 1, 3, and 5 wt%) after EB irradiation at doses of 0 and 25 kGy are shown in Fig. 5a, b.

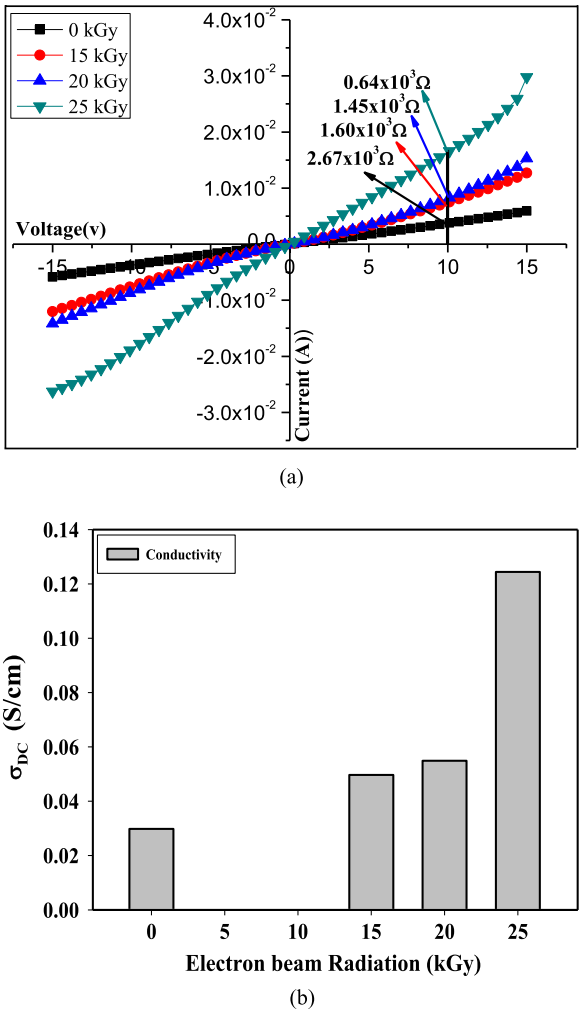

Fig. 4 **a** I–V curve of (XLPE/5-ZnO) and **b** the curve shows the electrical conductivity of zinc oxide (ZnO) nanoparticles (NPs) obtained at different electron beam doses (i.e., 0, 15, 20, and 25 kGy)

The conductivity of XLPE is also affected by the concentration of ZnO NPs. As shown in Fig. 5a, the conductivity of XLPE increased as the ZnO content increased with an irradiation dosage of 0 kGy. The inclusion of filling ZnO NPs in the insulator polymer of the XLPE system can transform it into a good conductor, allowing electrons to delocalize within the entire XLPE chains. Within the XLPE chains, the delocalized electrons move around nearly freely, functioning as conductive charge carriers. XLPE chains can be transformed to pose conductivity by allowing electrons to freely transfer between bonds. The filling procedure using ZnO NPs improves the conductivity of XLPE chains, which are normally nonconductive. ZnO NPs allow electrons to flow to a conductive gap,

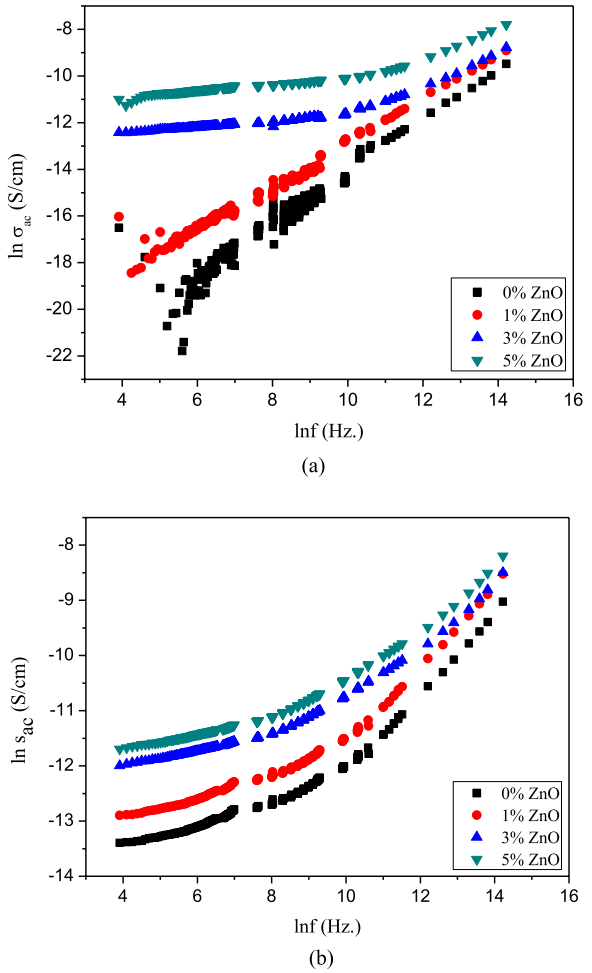

Fig. 5 Frequency dependence of alternating current (AC) conductivity for zinc oxide (ZnO) nanoparticle-filled (i.e., 0, 1, 3, and5%) cross-linked polyethylene at 0 kGy (**a**) and 25 kGy (**b**). The AC conductivity increases as the frequency increases due to the effects of the electron beam dose (25 kGy)

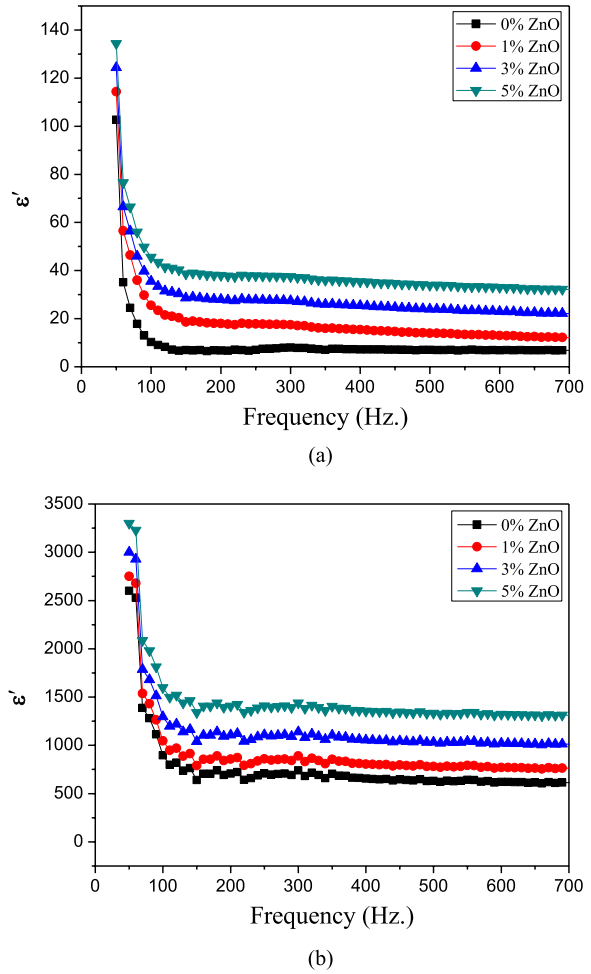

Fig. 6 Frequency dependence of dielectric constant ε' for zinc oxide nanoparticle-filled (i.e., 0, 1, 3, and 5%) cross-linked polyethylene irradiated at 0 and 25 kGy

allowing electrons to move throughout the polymer chain. When electrons transfer along a polymer chain, an electrical current is produced. Figure 5a suggests that the conductivity of (XLPE/ZnO) nanocomposite material changes exponentially at ZnO content of 3 and 5%, it is corresponding to the distance between two particles will decline, this will lead to the conductivity of composite materials increasing, whereas the content of ZnO at 0 and 1% has low conductivity due to the value of mass fraction of filler not reaching to the percolation threshold (Liu et al. 2019). Figure 5b shows that with increasing radiation doses, the conductivity of the XLPE/ZnO nanocomposite film increases. The experimental AC conductivity data of XLPE/ZnO nanocomposites showed that increasing the irradiation dosage significantly increases the AC conductivity, implying that the irradiation process improves the electrical properties of XLPE/ZnO nanocomposites. The structure of XLPE may be affected by EB irradiation. Depending on the dose, the cross-linked interaction between the XLPE chains changes the physical and chemical characteristics. Figure 5b shows that all samples of (XLPE/ZnO) nanocomposite material have exponentially increment after irradiation process the conduction process of XLPE/ZnO) nanocomposite will not depend on the contacting area between two ZnO nanoparticles, and it only depends on the electrons hopping process between two ZnO nanoparticles. Therefore, the current density which flows through the (XLPE/ZnO) nanocomposite could be enhanced by electron beam irradiation process.

Dielectric constant and loss factor for irradiated XLPE/ZnO nanocomposites

The dielectric constant results of XLPE/ZnO irradiated with EB at 0 and 25 kGy at different ZnO contents (i.e., 0, 1, 3, and 5 wt%) are shown in Fig. 6a, b. This figure shows that as the frequency increases, the dielectric constant decreases. El-Nahass et al. (2013) have observed the same behavior. Note that after frequencies of 125 Hz, the permittivity of the blank XLPE/ZnO nanocomposite sample was frequency-independent. This is because at low frequencies, charge carriers respond quicker to an externally applied electric field, resulting in a higher ε' value. Moreover, charge carriers at high frequencies could not keep up with the fast changes in the applied electric field, resulting in low ε' values. The reduction in the dielectric constant as the frequency of the applied field increases might be explained by several types of polarization (i.e., ionic, orientation, and electronic). Ionic polarization occurs when a material is exposed to an electric field, where positive ions move away from negative ions. This polarization intervenes for frequencies smaller than terahertz. Orientation polarization occurs in frequencies ranging between 100 and 450 Hz and is linked to the material structure. The permanent dipoles of the molecules are oriented toward the direction of the applied field in the presence of an applied field. Electronic polarization occurs because the electron cloud of an atom is displaced from its nucleus and all the electrons around it. This type of polarization occurs in a matter of seconds and is sensitive to frequencies well beyond those of visible light (10^{15} Hz). Orientation polarization is popular because it takes longer than other polarizations. As a result, ε' decreases until it approaches a constant value at a higher frequency, which corresponds to interfacial polarization. It has a greater dielectric constant than many other aromatic organic polymers, making it a suitable semiconductor material (Bouaamlat, et al. 2020). In contrast, with the irradiated XLPE/ZnO nanocomposite, the real part of permittivity rose substantially. This is because irradiation contributes to greater allowable charge transfers between molecules in case of a cross-linked structure. It could be predicted that cross-linking at a dosage of 25 kGy results in ZnO NP interconnections and partial polarity elevated by generated radical defects caused by irradiation of materials in the air environment (Suljovrujic 2010). Due to partial interconnections between ZnO NPs at filler concentrations more than 5 wt%, an increase in the real portion of permittivity at a raised ZnO content affects the dielectric behavior. Figure 6a, b shows the effects of EB irradiation and the filler content on AC conductivity. As predicted, the concentration of the conductive filler rose, increasing the irradiated XLPE/ZnO nanocomposite samples. The electrical conductivity of irradiated XLPE/ZnO nanocomposites increased by 24 orders of magnitude at the highest ZnO nano-filler content (the value of permittivity was 135 for non-irradiated XLPE/ ZnO nanocomposites with 5 wt% ZnO content (3300), indicating that the percolation threshold had been reached due to the development of a network of the conductive filler).

Figure 7 shows the variations in dielectric loss ε'' with frequency for irradiated XLPE/ ZnO nanocomposites at different ZnO contents (i.e., 0, 1, 3, and 5 wt%) upon EB irradiation at 0 and 25 kGy. The dielectric loss factor ε'' of non-irradiated and irradiated XLPE/ZnO nanocomposites. It is because when the frequency rises, the dipolar molecules in the XLPE polymer can respond to the rising rates of the applied field. Interfacial polarization causes the observed increase in dielectric loss ε'' in the low-frequency region (Rajendran et al. 2004). The trend is comparable in both non-irradiated and irradiated

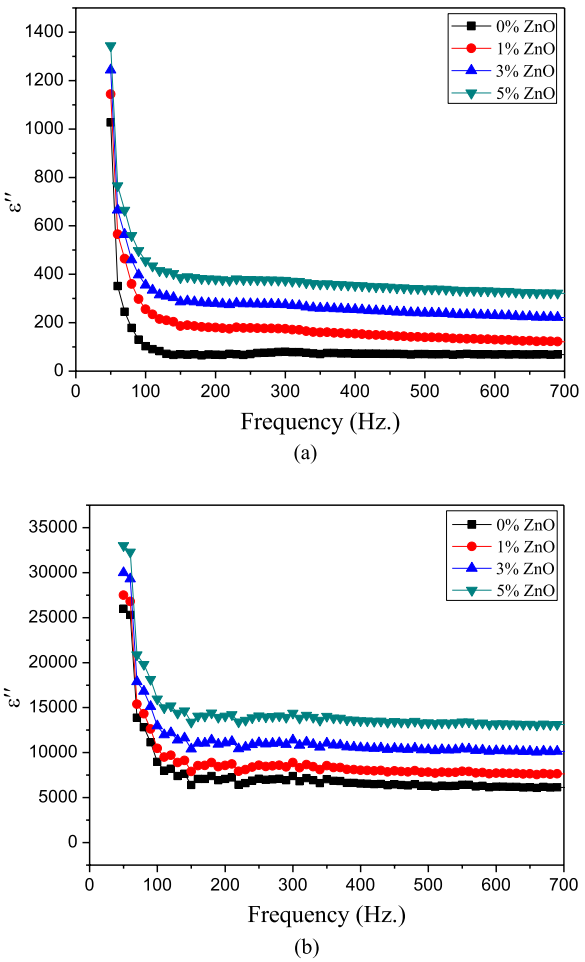

Fig. 7 Frequency dependence of dielectric loss ε'' for zinc oxide nanoparticle- filled (i.e., 0, 1, 3, and 5%) irradiated cross-linked polyethylene at 0 kGy (**a**) and 25 kGy (**b**)

XLPE/ ZnO nanocomposite samples. Figure 7a, b shows an increase in ε'' values with increasing EB dosage. This is due to the presence of charge carriers trapped in the polymer's band gap (Velitchkova et al. 2000).

Simulation and modeling of electric field distribution inside irradiated XLPE/5-ZnO nanocomposites at 25 kGy

The electric field distribution in MV cables was simulated using COMSOL Multiphysics. The distribution of electric fields inside XLPE-marked cables is shown in Fig. 8. The distribution of electric fields inside XLPE-marked cables was non-uniform at 1-mm arc length (Fig. 8). The electric field distribution for the XLPE/5-ZnO nanocomposite sample started to become uniform and gradually decreased from the inside to the outside (Fig. 9). This is because ZnO NP-filled XLPE maintained a uniform electrical field and reduced electrostatic stress. Figures 10 and 11

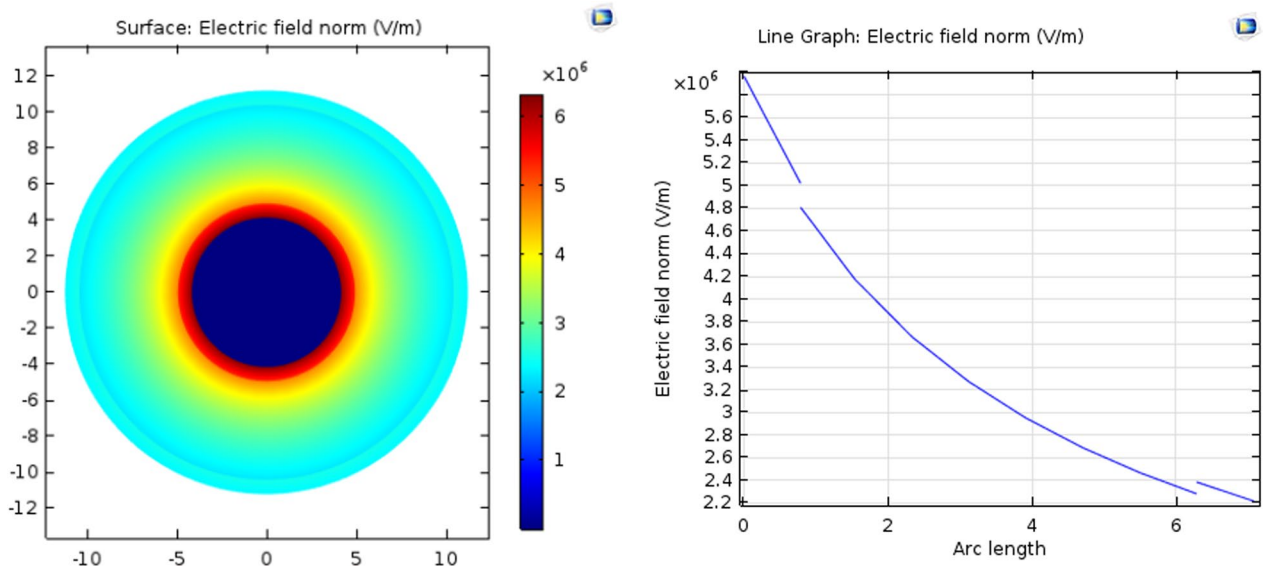

Fig. 8 Electric field distribution in medium-voltage (MV) cross-linked polyethylene-marked cables without zinc oxide filling

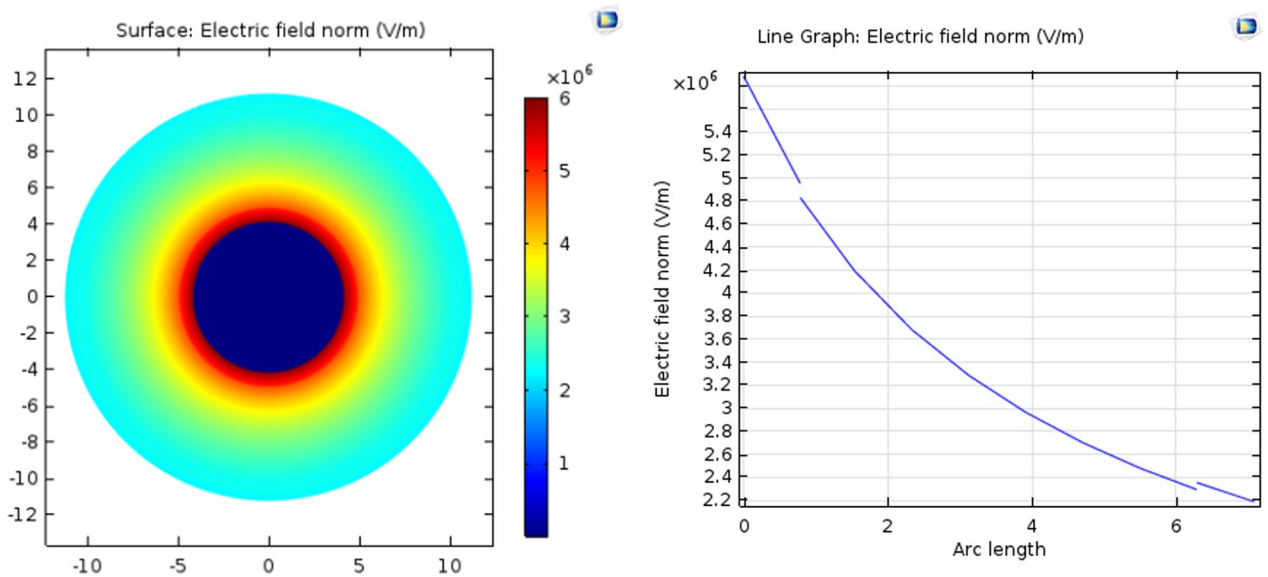

Fig. 9 Electric field distribution in medium-voltage (MV) cables with zinc oxide (ZnO) filling of polyethylene/5-ZnO irradiated at 25 kGy

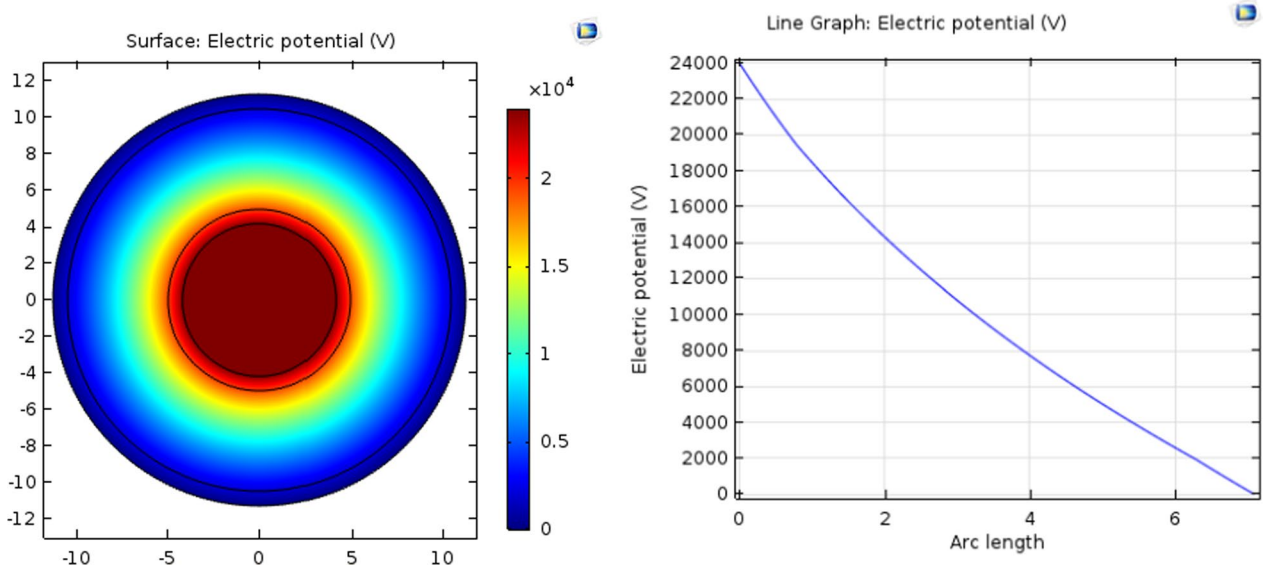

Fig. 10 Electric potential distribution in medium-voltage (MV) cross-linked polyethylene-marked cables without zinc oxide (ZnO) filling

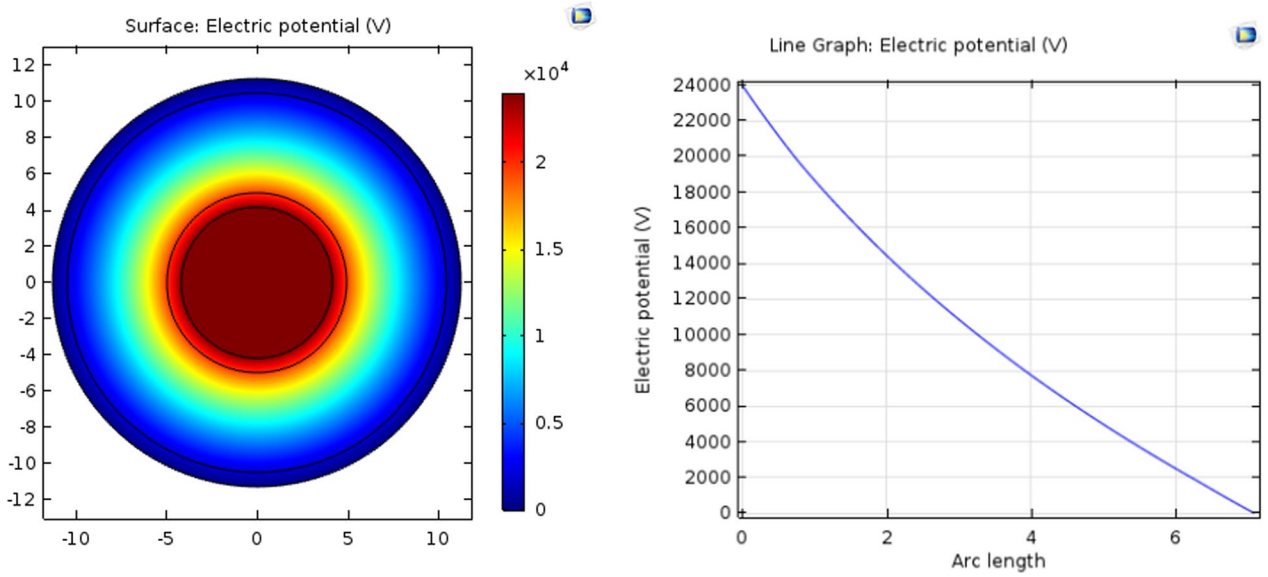

Fig. 11 Electric potential distribution in medium-voltage (MV) cables with zinc oxide (ZnO) filling of cross-linked polyethylene/5-ZnO irradiated at 25 kGy

show the distribution of electric potential in XLPE-marked cables and XLPE/5-ZnO nanocomposite samples, without changes in the behavior curve. For two samples, the electric potential distribution gradually decreased from 24,000 to 0 V.

Conclusion

The maximum uniform electric field was found in the middle of the XLPE/5-ZnO 25 kGy film sample, rather than at the top or bottom, according to the results. This might be attributed to a significantly low relative permittivity of

the new XLPE/5–ZnO 25-kGy film cable. COMSOL Multiphysics was used to investigate the distribution of the electric field in XLPE/ ZnO NP MV cable insulation under the impacts of the radius and relative permittivity. The ZnO NPs obtained were classified using TEM. The synthesized ZnO NPs were semi-spheres with sizes of 35–55 nm on TEM images. The band gap increased as the oxidation increased from 3.12 to 3.3 eV. The DC conductivity increased as the EB irradiation increased from 2.98×10^{-2} to 12.44×10^{-2} S/m. At low frequencies approaching 120 Hz, the dielectric constant ε' and dielectric loss ε' of non-irradiated and irradiated XLPE/ ZnO nanocomposite samples were high, and their values increased after the EB irradiation process. The AC conductivity of the polymer under study increased as the frequency and EB irradiation increased. The ZnO NP-filled XLPE maintained a uniform electrical field distribution and decreased electrostatic stress. The optimum AC/DC conductivity (AC: 1×10^{-4} S/m and DC: 12.44×10^{-2} S/m) in the minimum relative permittivity (2.24) was achieved for XLPE/ 5-ZnO with a ZnO NP content of 5 wt% irradiated at 25 kGy. COMSOL Multiphysics was used to simulate the electric field distribution within the MV cable of XLPE 5-ZnO irradiated at 25 kGy. Therefore, it is recommended that the XLPE market should be modified by adding ZnO NPs (5 wt%) and EB irradiated at 25 kGy. In producing scientific goods, the synthesis of ZnO NPs is of considerable importance.

Acknowledgements
We wish to thank gratefully National Centre for Radiation Research and Technology (NCRRT), Egyptian Atomic Energy Authority (EAEA), for the encouragement by providing the necessary facilities. We are also thankful to all staff members of Solid state and accelerator Department, NCRRT, for their support and appreciated help.

Author contributions
AIS, SAF, AFAEG, MAF, MII, and MMG shared equally in writing the manuscript and accepted the responsibility of the entire contents of this manuscript and approved the submission. All authors read and approved the final manuscript.

Funding
There was no external funding for this manuscript.

Availability of data and materials
Not applicable.

Declarations

Competing interests
The authors declare that they have no conflict of interest.

Author details
[1]Solid State and Accelerator Department, National Center for Radiation Research and Technology (NCRRT), Egyptian Atomic Energy Authority (EAEA), Cairo, Egypt. [2]Faculty of Engineering, Zagazig University, Zagazig, Egypt. [3]Radiation Research of Polymer chemistry department, National Center for Radiation Research and Technology (NCRRT), Egyptian Atomic Energy Authority (EAEA), Cairo, Egypt.

Received: 3 February 2022 Accepted: 11 May 2022
Published online: 24 May 2022

References

Aljoumaa K, Allaf AW. Morphology, structure, properties and applications of XLPE. In: Crosslinkable polyethylene (Springer, 2021). p. 125–166.
Bouaamlat H, et al. Dielectric properties, AC conductivity, and electric modulus analysis of bulk ethylcarbazole-terphenyl. Adv Mater Sci Eng. 2020. https://doi.org/10.1155/2020/8689150.
El-Nahass M, et al. AC conductivity and dielectric characterization of synthesized pN, N dimethylaminobenzylidenemalononitrile (DBM) organic dye. Vacuum. 2013;91:14–9.
Fattahi H, Pak A. Investigation of ultrasonic assisted electro discharge machining with TiO2, Al2O3 and ZnO Nano-powder. Amirkabir J Mech Eng. 2018;50(3):541–50.
Fayek S, et al. Study of γ-rays changes of the ZnO thin film structural and optical properties. Arab J Nucl Sci Appl. 2018;51(1):204–14.
Garino N, et al. Zinc oxide nanocrystals as a nanoantibiotic and osteoinductive agent. RSC Adv. 2019;9(20):11312–21.
Ghobashy MM, Alkhursani SA, Madani M. Radiation-induced nucleation and pH-controlled nanostructure shape of polyaniline dispersed in DMF. Polym Bull. 2018a;75(12):5477–92.
Ghobashy MM, et al. Radiation induced in-situ cationic polymerization of polystyrene organogel for selective absorption of cholorophenols from petrochemical wastewater. J Environ Manage. 2018b;210:307–15.
Ghobashy MM, et al. Characterization of Starch-based three components of gamma-ray cross-linked hydrogels to be used as a soil conditioner. Mater Sci Eng B. 2020;260:114645.
Ghobashy MM, et al. Controlling radiation degradation of a CMC solution to optimize the swelling of acrylic acid hydrogel as water and fertilizer carriers. Polym Adv Technol. 2021;32(2):514–24.
Hezam A, et al. Direct Z-scheme Cs 2 O-Bi 2 O 3–ZnO heterostructures for photocatalytic overall water splitting. J Mater Chem A. 2018;6(43):21379–88.
Janotti A, Van de Walle CG. Fundamentals of zinc oxide as a semiconductor. Rep Prog Phys. 2009;72(12):126501.
Kim C, et al. Investigation on dielectric breakdown behavior of thermally aged cross-linked polyethylene cable insulation. Polym Test. 2019;80:106045.
Ko SC, et al. Micromachined piezoelectric membrane acoustic device. Sens Actuators A Phys. 2003;103(1–2):130–4.
Kumar LS, et al. Synthesis of calcite-zincite nano composite materials using sol-gel auto combustion method. IOP Publishing. 2020.
Labuayai S, Promarak V, Maensiri S. Synthesis and optical properties of nanocrystalline ZnO powders prepared by a direct thermal decomposition route. Appl Phys A. 2009;94(4):755–61.
Lei W, et al. Are nano-composites really better DC insulators? A study using silica nanoparticles in XLPE. IEEE Trans Dielectr Electr Insul. 2017;24(4):2268–70.
Liu C, et al. Review of nonlinear conductivity theory research of modified composite materials. IEEE Access. 2019;7:50536–48.
Mahmood N, et al. Maximum piezoelectricity in a few unit-cell thick planar ZnO—a liquid metal-based synthesis approach. Mater Today. 2021;44:69–77.
Makhado E, et al. Sequestration of methylene blue dye using sodium alginate poly (acrylic acid)@ ZnO hydrogel nanocomposite: kinetic, isotherm, and thermodynamic investigations. Int J Biol Macromol. 2020;162:60–73.
Mohammed AJ, Hassan TAA. A new piezo-amperometric sensing method based on comb-like nanostructured zinc oxide thin films for the efficient detection of Na2SO4. Energy Procedia. 2019;157:1191–201.
Moniri S, et al. Synthesis and optical characterization of copper nanoparticles prepared by laser ablation. Bull Mater Sci. 2017;40(1):37–43.
Morshedian J, Mohammad HP. Polyethylene cross-linking by two-step silane method: a review. 2009.
Mututu V, et al. An investigation on structural, electrical and optical properties of GO/ZnO nanocomposite. Int J Electrochem Sci. 2019;14(3752–3763):3752.

Oliveira GL, Costa MF. Optimization of process conditions, characterization and mechanical properties of silane crosslinked high-density polyethylene. Mater Sci Eng A. 2010;527(18–19):4593–9.
Patil SK, Shinde SS, Rajpure KY. Physical properties of spray deposited Ni-doped zinc oxide thin films. Ceram Int. 2013;39(4):3901–7.
Pifferi V, et al. Photo-mineralization of noxious o-toluidine water pollutant by nano-ZnO: the role of the oxide surface texture on the kinetic path. Appl Catal B. 2015;178:233–40.
Prasad V, et al. Role of nanomaterials for forensic investigation and latent fingerprinting—a review. J Forensic Sci. 2020;65(1):26–36.
Raghu S, et al. Effect of electron beam irradiation on polymer electrolytes: change in morphology, crystallinity, dielectric constant and AC conductivity with dose. Radiat Phys Chem. 2014;98:124–31.
Raghu S, et al. Electron beam and gamma ray irradiated polymer electrolyte films: dielectric properties. J Radiat Res Appl Sci. 2016;9(2):117–24.
Rajendran S, Sivakumar M, Subadevi R. Investigations on the effect of various plasticizers in PVA–PMMA solid polymer blend electrolytes. Mater Lett. 2004;58(5):641–9.
Sharshir A, et al. Simulating the electric field distribution in medium-voltage cables of cross-linked polyethylene/Cu nanocomposites irradiated by E-beam with reference to the XLPE market. 2021. p. 1–12.
Simonenko EP, et al. Nanocrystalline ZnO obtained by the thermal decomposition of [Zn (H2O)(O2C5H7) 2] in 1-butanol: synthesis and testing as a sensing material. Russ J Inorg Chem. 2018;63(11):1519–28.
Singh A, Vishwakarma HL. Study of structural, morphological, optical and electroluminescent properties of undoped ZnO nanorods grown by a simple chemical precipitation. Mater Sci Poland. 2015;33(4):751–9.
Sree DN, et al. Enhanced UV light induced photocatalytic degradation of methyl orange by Fe doped spray pyrolysis deposited ZnO thin films. Appl Surf Sci. 2019;494:116–23.
Suljovrujic E. Dielectric study of post-irradiation effects in gamma-irradiated polyethylenes. Radiat Phys Chem. 2010;79(7):751–7.
Suwanboon S, et al. Physical and chemical properties of multifunctional ZnO nanostructures prepared by precipitation and hydrothermal methods. Ceram Int. 2014;40(1):975–83.
Thakur D, et al. Manganese-doped zinc oxide nanostructures as potential scaffold for photocatalytic and fluorescence sensing applications. Chemosensors. 2020;8(4):120.
Thomas J, et al. Recent advances in cross-linked polyethylene-based nanocomposites for high voltage engineering applications: a critical review. Ind Eng Chem Res. 2019;58(46):20863–79.
Velitchkova K, Krezhov K, Balabanov S. Temperature dependence of surface DC electrical conductivity of carbon-implanted polymers modified by gamma irradiation. Vacuum. 2000;58(2–3):531–5.
Wei J, Zhu L. Intrinsic polymer dielectrics for high energy density and low loss electric energy storage. In: Progress in polymer science, 2020: p. 101254.
Yılmaz S, et al. Defect-induced room temperature ferromagnetism in B-doped ZnO. Ceram Int. 2013;39(4):4609–17.
Younis SA, et al. Tailored functionalized polymer nanoparticles using gamma radiation for selected adsorption of barium and strontium in oilfield wastewater. Arab J Chem. 2020;13(2):3762–74.
Zaouk D, et al. Piezoelectric zinc oxide by electrostatic spray pyrolysis. Microelectron J. 2006;37(11):1276–9.

Publisher's Note